RESEARCH ARTICLE

Synthesis, Structures, and Properties of Terphenyl Diamido Complexes of Cobalt(I)

Suiho Kobayashi,[a] Yuka Yamada, [a] Tsubasa Hatanaka,*, [a] Motohiro Nakano,[b] and Yasuhiro Funahashi*, [a]

[a] S. Kobayashi, Y. Yamada, Prof. Dr. T. Hatanaka*, Prof. Dr. Y. Funahashi*
Department of Chemistry, Graduate School of Science, Osaka University
1-1 Machikaneyama, Toyonaka, Osaka, 560-0043, Japan
E-mail: hatanakat13@chem.sci.osaka-u.ac.jp
E-mail: funahashi@chem.sci.osaka-u.ac.jp

[b] Prof. Dr. Motohiro Nakano
Research Center for Thermal and Entropic Science, Graduate School of Science, Osaka University
1-1 Machikaneyama, Toyonaka, Osaka, 560-0043, Japan

Supporting information for this article is given via a link at the end of the document.

Abstract: To obtain a novel type of low-coordinate, low-valent complexes of cobalt, we performed synthesis and reactions of cobalt complexes supported by TDA^R ligands, which possess highly electron-donating amide groups with a terphenyl framework. Synthesis of $TDA^RCo(I)$ complexes **3** and **4** was successfully achieved by reducing Co(II) precursors **1** and **2** with potassium graphite. X-ray crystallography revealed that the cobalt centers are located close to the central aromatic rings of the TDA^R ligands, and the reduction of Co(II) to Co(I) strengthens this Co–arene interaction. Reaction of the cobalt(I) complexes with pyridine or DMAP provided N-donor ligated complexes **5** and **6**. Surprisingly, the Co–aromatic ring interactions in these complexes were found to be even stronger than those in **3** and **4**. These interactions with the aromatic rings were investigated in detail using computational methods.

Introduction

Monovalent cobalt species are among the most promising chemical species in the field of small molecule transformations mediated by first-row transition metals,[1] with numerous stoichiometric and catalytic reactions having been reported.[2] These reactions were typically achieved using *in situ* generated Co(I) species by the action of simple cobalt(II) salts and Grignard reagents or well-defined Co(I) complexes bearing phosphines or carbonyls as ancillary ligands. While understanding the full mechanistic scenario of these reactions opens pathways to improving the established reactions and discovering novel reactions, studying the true reactive species—coordinatively unsaturated Co(I)—poses considerable difficulties. This is due to the fact that such reactive Co(I) species are generally high-spin paramagnetic compounds, making their characterization difficult unless isolated as crystals. Furthermore, stabilizing their low-coordinate states to prevent aggregation or decomposition is challenging, and their extreme sensitivity to air and moisture further complicates isolation. Thus, while elucidating the properties and reactivity of coordinatively unsaturated Co(I) species is a compelling goal, their full nature and behavior remain largely unraveled in the field.

Bulky anionic amide ligands are known to be useful for facilitating the synthesis of low-coordinate transition metal complexes.[3] However it is only in recent years that the synthesis of low-valent cobalt amide complexes has been unveiled, beginning with the 2014 work of G. J. Long and P. P. Power *et al.* on $[Co\{N(SiMe_3)Dipp\}_2]^-$ (Dipp = 2,6-diisopropylphenyl).[4] Since then, (NHC)Co{N(Ar*)($SiPh_3$)} (NHC = :C{N(^{i}Pr)C(Me)}$_2$, Ar* = $C_6H_2\{C(H)Ph_2\}_2Me$),[5] $[Co\{N(SiMe_3)_2\}_2]^-$,[6] (IPr)Co{N($SiMe_3$)$_2$} (IPr = :C{N(Dipp)C(H)}$_2$),[7] $[Co(TIPSDAX)]^-$ (TIPSDAX: xanthene-based tridentate NON ligand),[8] (IPr)Co{N($SiMe_3$)Dipp},[9] and $[Co\{N(SiMe_2R)Dipp\}_2]^-$ (R = Ph, allyl)[10] have been reported, except for amide complexes stabilized by π-acidic phosphine ligands. Notably, the extensive studies by Werncke group have recently shed light on the reactivity of the cobalt(I) bisamide complexes.[10,11] These investigations are invaluable as they provide new insights into small molecule activation using low-coordinate cobalt(I) centers.

To further expand the scope of this class of compounds, we decided to employ a terphenyl diamide (TDA^R) ligand (Figure 1), which features a terphenyl backbone with two amide groups, and bulky aryl substituents, Mes (2,4,6-trimethylphenyl) or Dipp, attached to the nitrogen atoms. The electronic properties of $[TDA^R]^{2-}$ (R = Mes, Dipp) render the cobalt center electron-rich, owing to the strong electron-donating ability of the amide groups. In terms of steric characteristics, the bulky aryl substituents kinetically stabilize the coordinatively unsaturated cobalt center by preventing undesired dimerization through bridging by the amide ligands. Most notably, the central aromatic ring of the terphenyl skeleton can weakly coordinate to the cobalt center by using its π- or π*-orbitals, providing slight stabilization of the low-coordinate metal center. These features are expected to facilitate the synthesis and isolation of reactive, low-coordinate cobalt(I) complexes supported by amide ligands.

Herein, we describe the synthesis of novel low-coordinate Co(I) complexes supported by terphenyl-based bisamide ligands, which were characterized through crystallographic, electrochemical, magnetochemical, and computational studies. Additionally, we briefly examine their reactivity with N-donor ligands, highlighting the potential versatility of these cobalt(I) complexes in coordination chemistry.

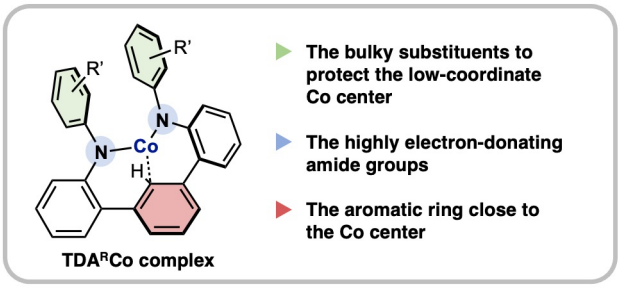

Figure 1. Important features of TDA^R ligand.

Results and Discussion

Synthesis of the H_2TDA^{Mes} ligand using Buchwald–Hartwig coupling reaction[12] has been previously reported by A. S. Veige *et al*.[13] Modifying the synthetic procedure, we prepared the ligands H_2TDA^R (R = Mes, Dipp). Specifically, terphenylene dibromide[14] was allowed to react with trimethyl or diisopropyl aniline in toluene at 100 °C to provide H_2TDA^R, which were isolated in 70% yield for R = Mes and 37% yield for R = Dipp, respectively. The NMR features of TDA^R are indicative of highly symmetric structures, as only one set of aryl and terphenyl resonances are present (Figure S1, S2).

The reaction of H_2TDA^R with a strong base $KN(SiMe_3)_2$ and cobalt chloride followed by addition of 15-crown-5 ether afforded anionic $[(TDA^R)Co^{II}Cl]^-$ complexes **1** and **2**, respectively (Scheme 1). A similar procedure without crown ether provided neutral $(TDA^R)Co^{II}(THF)$ complexes **1′** and **2′**, in which a THF molecule coordinates cobalt center instead of the chloride ion. Notably, it was difficult to obtain these THF complexes with both good yield and purity, and unoptimized crystallization always resulted in a mixture containing a white powder, presumed to be KCl.

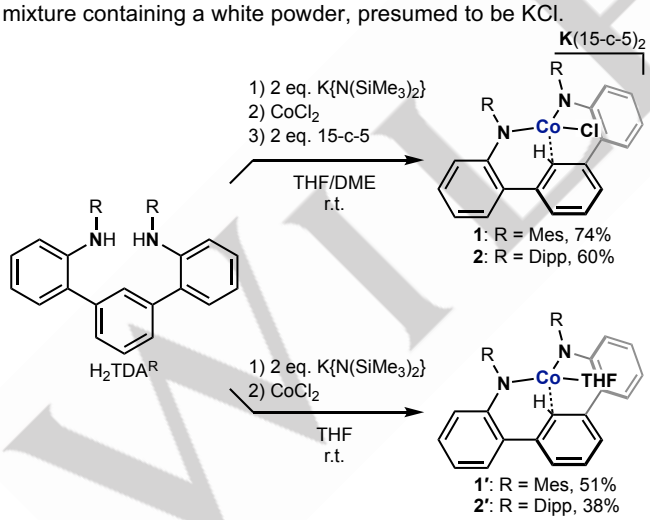

Scheme 1. Synthesis of cobalt(II) complexes having TDA^R, where R = 2,4,6-trimethylphenyl (Mes) or 2,6-diidopropylphenyl (Dipp). 15-c-5 denotes 15-crown-5 ether.

X-ray crystallography revealed that all four complexes have monomeric structures supported by two amide groups of $[TDA^R]^{2-}$ ligand and one chloride ion for **1** and **2** or one THF molecule for **1′** and **2′** (Figure 3, S6, S10, S13, S15). In the chloride complexes **1** and **2**, potassium ions are captured by two 15-crown-5 ether molecules and have no marked interactions with the anionic $[TDA^RCo^{II}Cl]^-$ part. Most notably, the central arene rings coordinates to cobalt centers in η^1-fashion as represented by the Co–C distances of 2.3243(16) Å (**1**), 2.312(3) Å (**1′**), 2.347(4) Å (**2**), and 2.302(2) Å (**2′**) (Table 1, S1), which are typical bond lengths for the Co(II) π-arene complexes with η^1- or η^2-fashion.[15] Including the Co–C interaction, each of the cobalt centers adopts four-coordinate, distorted tetrahedral structures where τ_4 values[16] are 0.88 (**1**), 0.86 (**1′**), 0.79 (**2**), and 0.72 (**2′**), respectively. The Co–N(amide) bond lengths of 1.9395(15), 1.9690(15) Å (**1**), 1.902(2), 1.923(2) Å (**1′**), 1.939(3), 1.969(3) Å (**2**), and 1.913(2), 1.935(2) Å (**2′**) are comparable to those of previously reported 3-coordinate cobalt(II) bisamide complexes such as $[CoX\{N(SiMe_3)_2\}_2]^-$ (X = F, Cl, Br) (1.923(2)–1.935(4) Å),[11f,11g,17] $[CoBr\{N(Dipp)SiMe_3\}_2]^-$ (1.914(2), 1.917(2) Å),[11f] $Co\{N(SiMe_3)_2\}_2(THF)$ (1.9000(15) Å),[18] and $Co\{N(SiMe_2Ph)_2\}_2(THF)$ (1.9219(10), 1.9251(10) Å).[19]

To assess the accessibility of Co(I) species, we conducted cyclic voltammetry on the Co(II) complexes **1**, **2**, **1′**, and **2′**. The THF complexes **1′** and **2′** exhibited reversible redox processes in the negative side, respectively (Figure 2). The waves at $E_{1/2}$ = 2.15 V (**1′**) and 1.96 V (**2′**) versus $Fc^{+/0}$ is assignable to the Co^{II}/Co^{I} redox couple, indicating the reduced derivatives of **1′** and **2′** are chemically accessible. In contrast, the anionic chloride complexes **1** and **2** showed no obvious redox waves within the measurable range on the negative side (Figure S7, S11), likely due to their formal charge of –1, which results in electron enrichment at the cobalt centers.

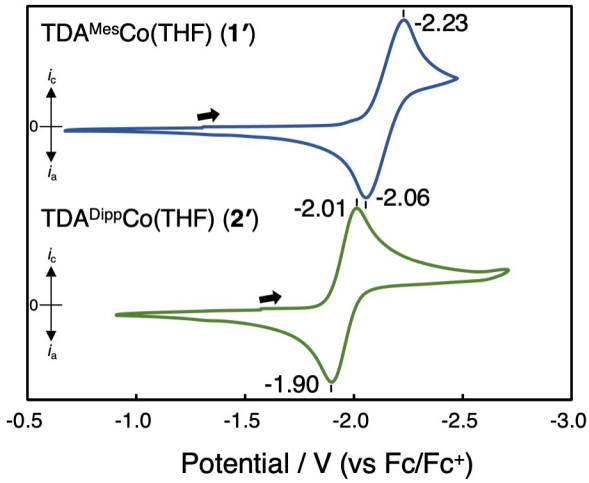

Figure 2. Cyclic voltammograms of **1′** and **2′** in a THF solution of 0.2 M $[^nBu_4N][PF_6]$ as the supporting electrolyte, with Au working electrode.

According the results of cyclic voltammetry, we carried out chemical reduction of the Co(II) complexes. Despite differences in redox behaviors between the chloride and THF complexes, reduction of all the Co(II) complexes with 1 equivalent of KC_8 was found to afford cobalt(I) complexes **3** or **4** in good yields, respectively (Scheme 2). The fact that reduction of **1** and **2** was possible despite no clear redox events in the CV indicates that the potassium atom assists dissociation process of chloride anion from the cobalt center. As a side note, synthesis of these Co(I) complexes from the H_2TDA^R ligands, without isolation of the Co(II) complexes, was also performed, allowing isolation of the desired complexes in high yields of 74% for **3** and 84% for **4**, respectively

(see Experimental in Supporting Information). ^{1}H NMR spectra of **3** and **4** showed paramagnetically shifted signals (Figure S16, S22), clearly suggesting high-spin (S = 1) configuration of Co^{I} atoms while common cobalt(I) complexes have low-spin (S = 0) configuration due to presence of relatively strong π-back bonding. The temperature-dependent magnetic susceptibilities were investigated for solid-state of **3** and **4**, and magnetic moment of 1.62 to 4.08 μ_B for **3** and 2.27 to 5.11 μ_B for **4** were obtained at 2 to 300 K (Figure S17, S23). These values also obviously indicate that Co^{I}, d^8, high-spin, S = 1 electronic configuration is ground state. The larger μ_{eff} values at 300 K than spin-only value (μ_{SO} = 2.83 μ_B) are not uncommon for low-coordinate cobalt(I) complexes.[4–10,11e,11i]

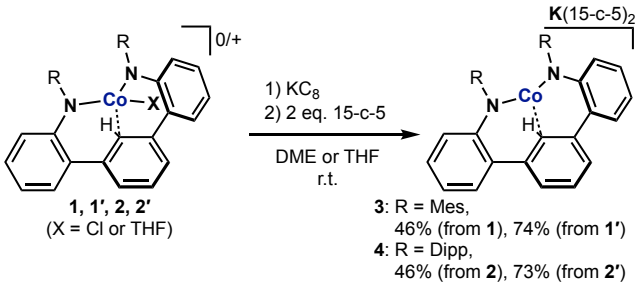

Scheme 2. Synthesis of TDA^R complexes of cobalt(I).

The solid-state structures revealed that the complexes **3** and **4** are monoanionic, with one potassium ions serving as a counter cation, solvated by two 15-crown-5 ether molecules, confirming that the complexes are indeed reduced. The cobalt centers in these complexes lack of coordination of THF molecule or chloride ions (Figure 3, S24), likely due to electron enrichment at cobalt center upon reduction. Such low coordination preference of Co(I) over Co(II) bis-amide complexes is well-documented in previous studies.[6a,7b,8,9] The coordination geometry around the cobalt centers adopts a planer T-shaped structures, with N1–Co–N2 bond angle of 169.22(7)° for **3** and 167.57(8)° for **4** (Table 1, S2, S3). As noted in the introduction, examples of two-coordinate Co(I) bisamide complexes are scarce while the Co–N distances of 1.8916(17), 1.8969(16) Å for **3** and 1.8762(19), 1.8893(17) Å for **4** are comparable to those reported in the literature (1.878(2)–1.8979(11) Å).[4,6,9e] The T-shaped geometry and the structural similarity to two-coordinate bisamide complexes suggest that the interaction with the aromatic ring is weak and does not notably influence to the cobalt–amide bond. However, contrary to expectations from such weak interactions, the one-electron reduction of cobalt strongly affects cobalt–aromatic ring interactions. This reduction shortens the Co–C distances (2.191(2) Å (**3**), 2.093(2) Å (**4**)) by approximately 0.1–0.2 Å compared to the corresponding Co(II) precursor, likely due to enhanced back-donation from the metal to the ligand. The shortened Co–C bond distances resemble that of the sole reported three-coordinate Co(I) complex featuring η^1-arene interaction (2.103(2) Å), as described by C. Jones *et al*.[5]

Although the condition is not yet clear, crystallization of complex **4** was found to sometimes yield crystals of a structurally different complex. The X-ray diffraction of the crystals exhibited that the complex, denoted as **4′**, possesses the almost similar structure but the position of cobalt is slightly shifted toward the center of the aromatic ring, depicted by superimposed structure in Figure 4. On the basis of the structures, the cobalt center in **4** was tentatively presumed to interact with C–H bond *via* agostic interaction (Co–H = 1.76(2) Å, Co–C = 2.093(2) Å) while in **4′** with π-orbitals in aromatic ring (Co···H = 2.31(3) Å, Co–C = 2.217(4) Å) (Table 2, S3). Since only former type complex was obtained regarding the complex **3** having Mes groups (Co–H = 1.90(2) Å, Co–C = 2.191(2) Å), bulky Dipp group possibly generates bistability system providing the two kinds of crystals. The details of interaction between the cobalt center and the central aromatic ring will be discussed later in theoretical study section.

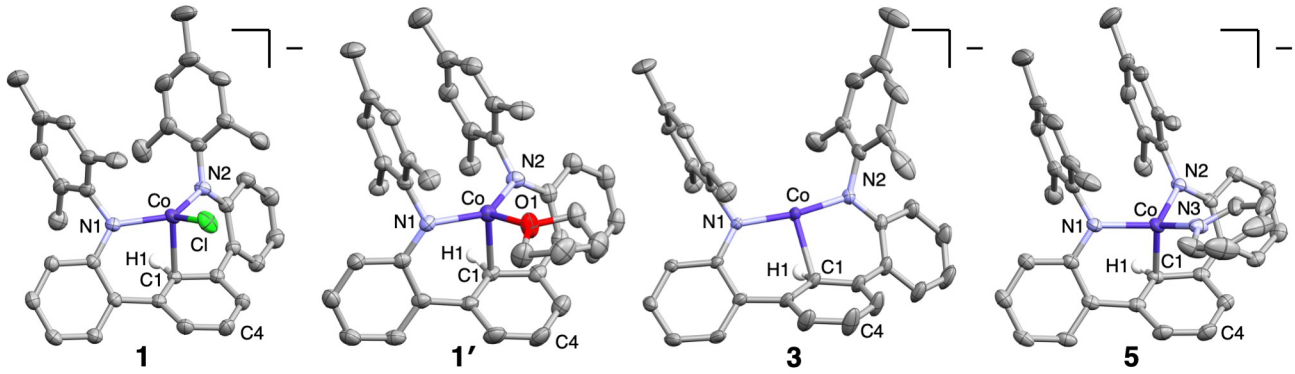

Figure 3. Solid-state structures of TDA^{Mes} Co(II) and Co(I) complexes **1**, **1′**, **3**, and **5** with thermal ellipsoid plots displayed at 50% probability level. For ionic compounds, only the anionic part is shown. All hydrogen atoms except for H1 and one of disordered pairs is omitted for clarity.

Table 1. Summary of selected bond distances /Å and angles /°. Experimental data collection was performed at 193 K for **1**, and 113 K for **3** and **5**.

	1: Exp.	**1**: Calc.	**3**: Exp.	**3**: Calc.		**3**[f]: Calc.	**5**: Exp.	**5**: Calc.	
		S = 3/2		S = 1	S = 0	S = 1		S = 1	S = 0
Co–N^{amide} /Å	1.9690(15)	1.96	1.8916(17)	1.91	1.87	1.88	1.9814(16)	1.99	1.90
	1.9395(15)	1.95	1.8969(16)	1.92	1.88	1.89	2.0294(16)	2.03	1.96
Co–N^{py} /Å							2.0097(18)	2.00	1.90
Co–Cl	2.2486(5)	2.28							
Co–C1 /Å	2.3243(16)	2.28	2.191(2)	2.19	1.91	2.08	1.9930(19)	2.01	2.00
Co–C1–C4 /°	105.34(8)	102.5	132.87(13)	101.5	154.7	138.5	100.60(9)	98.3	107.2

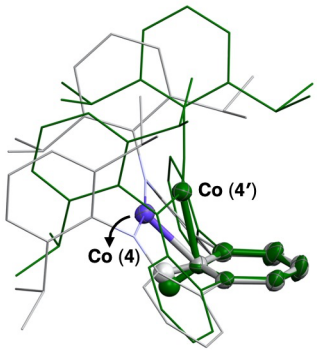

Figure 4. Structural overlay of **4** (coloured by elements) and **4′** (colored in green).

Table 2. Summary of selected bond distances /Å and angles /°.

	4	**4′**
Co–N^{amide} /Å	1.8893(17)	1.913(4)
	1.8762(19)	1.904(4)
Co–C1 /Å	2.093(2)	2.217(4)
Co–C1–C4 /°	138.17(11)	109.31(15)

In the Introduction section, we presented previous examples of low-coordinate, low-valent cobalt bisamide complexes. While certain properties of these complexes remain unclear, the complexes synthesized in this study exhibited two critical differences compared to the previously reported examples. First, whereas all previously reported Co(II)/Co(I) redox processes are irreversible,[4,6a] our complexes demonstrate high reversibility. Second, regarding thermal stability, $[Co\{N(SiMe_3)_2\}_2]^-$, due to its labile nature, gradually decomposes in solution at room temperature,[6b,11e] whereas the complexes synthesized in this study remain stable in solution at room temperature and show minimal changes even after heating at 65 °C for 72 hours. The exceptional redox behavior and thermal stability of our low-valent cobalt complexes with amide ligands are likely due to interactions with the central arene ring of the terphenyl framework. There are two illustrative examples of low-valent transition metal complexes stabilized by π-orbital of a terphenyl: Holland's bisthiolate complexes of Fe(–I)–Fe(II)[20] and Agapie's diphosphine complexes of Ni(0)–Ni(II).[21] Each study has shown that the interaction between the aromatic ring and the metal center changes flexibly depending on the oxidation state and coordination number of the metal center. When the metal center is in a low-valent state, the bond strength is enhanced by increased back-donation from the metal to the central aromatic ring. Our complexes exhibit a similar trend, suggesting that in the case of monovalent cobalt, stabilization occurs *via* back-bonding with the aromatic ring. This stabilizing effect enabled the facile isolation of the complex, even when the central metal became electron-rich due to the electron-donating amide ligands.

With the unique cobalt(I) complexes in hand, we explored the fundamental reactivities of them with donor ligands. Reaction of the complex **3** with pyridine (Py) or 4-dimethylaminopyridine (DMAP) allowed gradually color changes of solution from greenish brown to brown. From the reaction mixtures, N-donor coordinated cobalt(I) complexes, $[K(15\text{-c-}5)_2][(TDA^{Mes})Co^{I}(Py)]$ (**5**) and $[K(15\text{-c-}5)_2][(TDA^{Mes})Co^{I}(DMAP)]$ (**6**) were isolated as dark brown crystals, respectively (Scheme 3). Unfortunately, TDA^{Dipp} analogues were not isolated from the reaction of **4** with the N-donor ligands because of high solubilities of the products.

The complexes **5** and **6** still exhibited paramagnetic features in ^{1}H NMR (Figure S28, S33), and magnetic moments were determined to μ_{eff} = 3.99 μ_B (**5**) and μ_{eff} = 3.76 μ_B (**6**) at 300 K with SQUID magnetometry, indicating the high-spin d^8 configurations (Figure S29, S34).

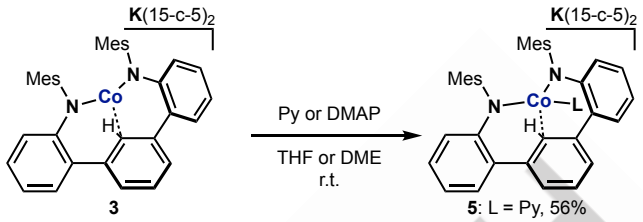

Scheme 3. Reactions of the $TDA^{Mes}Co(I)$ complex **3** with pyridine (Py) or 4-dimethylaminopyridine (DMAP).

X-ray analysis exhibited that one pyridine or DMAP molecule coordinates to the cobalt center providing pseudo tetrahedral geometry around the cobalt centers (τ_4 = 0.87 (**5**), 0.80 (**6**)) (Figure 3, S35). To the best of our knowledge, only square planar complexes have been reported for Co(I) complexes having pyridines, and no appropriate example for comparison exists but the Co–N(donor) distances (2.0097(18) Å, 2.038(2) Å) in the complex **5** and **6** (Table 1, S4, S5) are slightly longer than those of the known complexes such as $[\{bis(iminoethyl)pyridine\}Co^{I}(Py)]^+$ (Co–N(Py): 1.946(3) Å)[22] and $\{^{Mes}CCC\}Co(Py)$ (^{Mes}CCC = bis(mesityl-benzimidazol-2-ylidene)phenyl) (Co–N(Py): 1.962(3) Å).[23] This difference in the bond lengths arises from the spin states, with the bonds being longer in the present complexes due to their high-spin state. Generally, increase of coordination number makes the metal–ligand bond longer because of electron enrichment of the metal center. In contrast, the distances between the cobalt atom and the carbon atoms (C1) of the central aromatic ring in the complexes **5** (1.9930(19) Å) and **6** (1.961(3) Å) become significantly shorter than that in the precursor complex **3** (2.191(2) Å). Reflecting the strong interaction, the bond lengths between C1 and its adjacent carbon atoms are elongated by approximately 0.03–0.05 Å compared to those in complex **3** (Figure S36). Curiously, the Co–C distances are also shorter than the reported Co–C single bond lengths (1.996(2)–2.053(8) Å) in tetrahedral Co(I) or Co(II) aryl complexes.[24] Such strong cobalt–arene interactions are known only for polyaromatic complexes[25] or multinuclear Co(I) complexes,[25d–f,26] where back-donation from metal to ligand is especially favored. On the other hand, the strong metal-aromatic interactions in the complexes **5** and **6** are intriguing in that they are achieved by a mononuclear cobalt center rendered electron-rich by the amide ligands.

To gain insights into the electronic structures, DFT calculations were performed for the Co(II) complex **1** bearing TDA^{Mes}, the Co(I) complex **3**, and its pyridine adduct **5**. A full description of the calculation methods employed can be found in the Supporting Information. Regarding **3** and **5**, the structural optimization was performed for both singlet and triplet states, and confirmed that the triplet states of complexes **3** and **5** were more stable than the singlet states by 19.1 and 21.2 kcal/mol, respectively (Figure S37). In triplet states of these complexes, the Co centers were in +1-oxidation states with a high-spin d^8 configuration, and the spin density was predominantly localized

on the cobalt (Figure S38). The high-spin preferences in these complexes are good agreement with the results from the SQUID measurements mentioned above.

The structural optimization closely reproduced the experimentally obtained structures for the Co(II) complex **1** and the pyridine complex **5**, including the Co–N bond lengths and the distance between the Co center and the carbon atom in the aromatic ring (Table 1). However, the computed structure for the complex **3** differed somewhat from the experimental data, particularly in the relative position of the cobalt center with respect to the central aromatic ring. Adopting the angle ∠Co–C1–C4 (C1, C4: carbons at the 1- and 4-positions of the central aromatic ring (Figure 5a)) as a parameter of the relative position, the experimental value was 132.87(13)°, while the optimized structure showed 101.5°. To investigate how the stability varies with the position of the cobalt center, a relaxed scan was performed by varying the ∠Co–C1–C4. Interestingly, the cobalt center was found to occupy relatively free positions on the aromatic ring without significant energy barriers or gaps. The potential energy surface took a broad double-well shape, with only a difference within *ca*. 2 kcal/mol in the Co–C1–C4 angle range of 80–150° (Figure 5b, black). This minimal energy difference suggests that the actual molecular structure in the solid state is likely influenced by relatively weak interactions, such as packing effects. Upon closer inspection of the crystal structure, the terphenyl moiety was found to be brought closer to the crown ether of the counter cation by C–H–π interactions (Figure S21), causing the mesityl group to bend slightly in the endo direction. Thus, by fixing the two C_a–C_b–N–C_c torsion angles (as defined in Figure 5a) corresponding to the endo bending to the experimental values and re-optimizing the structure, we successfully obtained the desired structure, designated as **3**$^{\mathbf{f}}$, that reproduces the experimentally obtained structure well (Table 1). Furthermore, partially relaxed scan holding this constraint yielded a broadly flat potential surface with a minimum at 138.5° (Figure 5b, red).

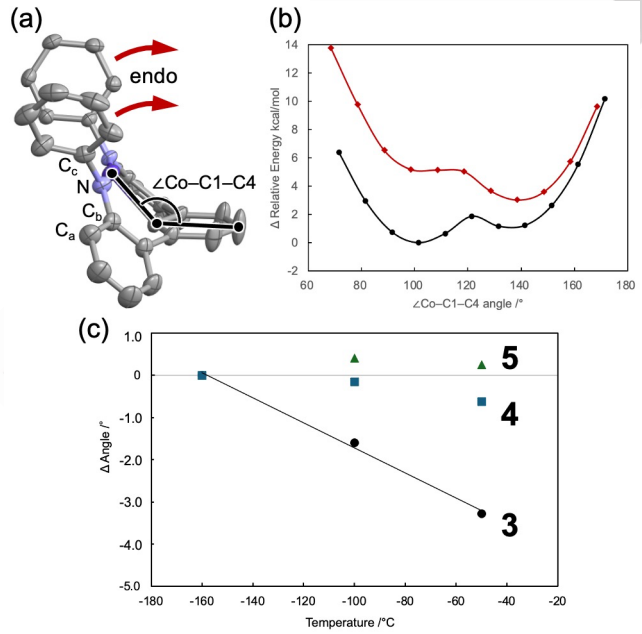

Figure 5. (a) Side-view of the molecular structure of **3**, depicting ∠Co–C1–C4. The methyl groups and the hydrogen atoms are omitted for clarity. (b) The fully relaxed (black) and partially relaxed (red) potential energy scans for the Co−C1−C4 angle. In the partially relaxed scan, two torsion angles corresponding bent of mesityl groups in the endo-direction were frozen. (c) experimentally observed ∠Co–C1–C4 in **3**–**5** at 113, 173, and 223K. Solid lines in (b) and (c) are shown as a guide to the eye.

To experimentally verify the fact that the cobalt center can move freely over the aromatic ring with minimal energy barriers, temperature-dependent single-crystal X-ray structure analyses were performed. If the asymmetric energy surface obtained from the calculation is correct, the average molecular structure observed by X-ray diffraction should change with increasing temperature (due to the asymmetric broadening of the probability distribution of accessible molecular conformations), leading to a decrease in the C–C–Co angle. Indeed, X-ray measurements at –160°C, –100°C, and –50°C confirmed that, as predicted, the position of the Co center shifted toward the center of the aromatic ring at higher temperatures in the TDA^{Mes} complex **3** (Figure 5c, for the details, see Figure S18–20, Table S2). In contrast, temperature-dependent measurements of the TDA^{Dipp} complex **4** (Figure S24–26, Table S3) and the pyridine complex **5** (Figure S30–32, Table S4) showed little change in the cobalt position. For the complex **4** and **5** in crystalline state, the energy barriers associated with changes in the Co–C1–C4 angle are likely relatively high, suggesting that the Co center cannot move noticeably within the accessible temperature range. This may also explain why two different crystalline forms **4** and **4′**, each with a different cobalt position, were obtained upon crystallization from solution. Specifically, in the case of **4**, the energy barrier at the center of the double-well potential is presumed to be relatively high, allowing it to be overcome in the solution state but not in the crystalline state.

Regarding the interaction between the cobalt center and the aromatic ring, QTAIM analysis[27] indicated the presence of bonding interactions, as evidenced by the observation of a bond critical point between Co and C (Figure 6). The Laplacian of the electron density ($\nabla^2\rho$) was 0.14 for **1**, 0.13 for **3**, and 0.13 for **5** (Table S7), suggesting ionic bonding. Additionally, Wiberg Bond Index (WBI)[28] and Mayer Bond Index (MBI)[29] further supported the presence of Co–C bonding (**1**: 0.35 (WBI), 0.25 (MBI), **3**: 0.45 (WBI), 0.33 (MBI), **5**: 0.62 (WBI), 0.51 (MBI)) (Table S8). The order of magnitude of the bond indices is consistent with the order of experimentally observed bond lengths. As mentioned above, based on the solid-state structure, the presence of a C–H agostic interaction was anticipated. However, QTAIM analysis revealed that, regardless of the position of the cobalt center, the interaction occurred primarily with the carbon atoms of the aromatic ring, and no interaction with the hydrogen atoms was found.

In this series of complexes, it is noteworthy that all bonds between the cobalt center and the ligands exhibit less covalent character. Consequently, orbital interactions corresponding to back-donation from the cobalt center to the aromatic rings were scarcely observed in the calculated molecular orbitals, except for one case discussed later (Figure S39, S40, S43, S44, S47, S48). To systematically evaluate the interaction between cobalt and the aromatic ring across the complexes, we performed second-order perturbation theory (SOPT) analysis[30] of the Fock matrix in NBO analysis. SOPT analysis provides insights for Lewis donor-acceptor interaction between NBOs, and is also useful for evaluating the degree of back-donation from metal to ligand. As a result, the analysis revealed that the donation from the aromatic ring to cobalt provides a stabilization energy of 2 kcal/mol (α spin) and 8 kcal/mol (β spin) in **1**, and 2 kcal/mol (α spin) and 9 kcal/mol (β spin) in **3** (Figure S42, S46). In contrast, stabilization energy

caused by the back-donation from cobalt to the aromatic ring is 2 kcal/mol (α spin) and 1 kcal/mol (β spin) for **1**, and 5 kcal/mol (α spin) and 4 kcal/mol (β spin) for **3** (Figure 7a). While all of these values are small for a stabilization energy, these findings clearly demonstrate that the reduction of the cobalt center significantly enhances the relative strength of the back-donation interaction. Notably, for **5**, the relative magnitudes of stabilization energies switch, with the stabilization from ligand-to-metal donation being 3 kcal/mol (α spin) and 4 + 4 kcal/mol (β spin) and that from metal-to-ligand donation reaching 9 kcal/mol (α spin) and 25 kcal/mol (β spin) (Figure 7a, S50). This means that coordination of the pyridine induces umpolung of the Co–aromatic ring interaction, allowing the aromatic ring to act as a weak Z-type ligand.[31] The β-spin metal-to-ligand electron donation was also observable in the molecular orbitals depicted in Figure 7b, which were primarily derived from a cobalt d orbital interacting with the aromatic ring's π* orbital. However, this molecular orbital has the highest energy among the molecular orbitals derived from the three occupied β d-orbitals, indicating that orbital stabilization through the metal-to-arene donation is limited even in the case of complex **5**. This computational result is quite unexpected, considering that the Co–C distances in the pyridine and DMAP complexes fall into the shortest category among the previously reported Co(I)–arene distances. The small stabilization energies for the cobalt–aromatic ring interactions observed in all of the complexes can be attributed to the low-coordinate, low-valent cobalt having d orbitals that are either doubly or singly occupied and energetically low-lying (an electronic factor), as well as the rigid coordination framework of the TDA ligand and the small ionic radius of cobalt (steric factors), both of which hinder effective interactions with the π or π* orbitals of the aromatic ring. As a result, in the ligand field provided to cobalt, the Co–arene interaction is considered to play a secondary role compared to the interactions with amide and pyridine ligands.

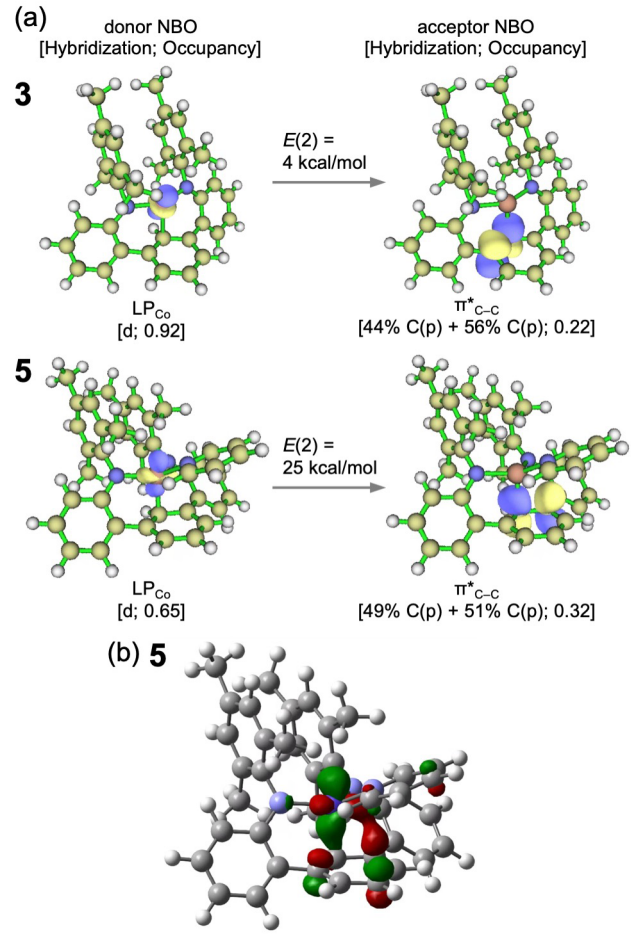

Figure 7. (a) Donor → acceptor NBO interactions in **3** and **5**, relevant to the back bonding of Co → aromatic ring. (b) HOMO (#166) of β molecular orbital of **5**.

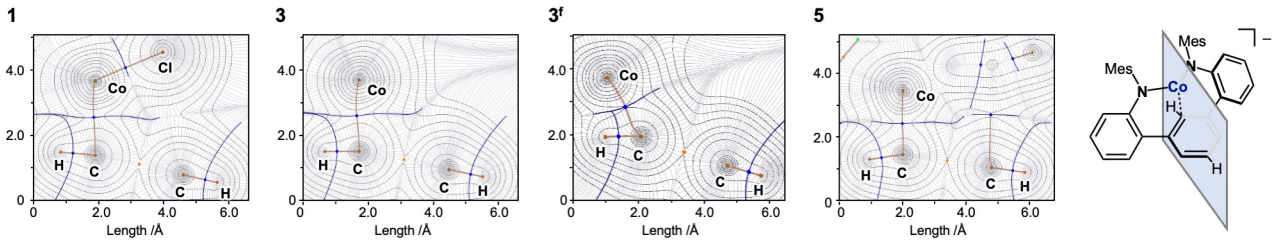

Figure 6. Topological QTAIM-derived plots of $\nabla^2\rho$ for **1**, **3**, **3**^{f} (constrained **3**), and **5**. Solid, black contours where $\nabla^2\rho > 0$. Blue dots are BCPs, orange dots are RCPs, brown bold lines are bond paths, and blue bold lines are interbasin paths.

Conclusions

In conclusion, we synthesized and reduced cobalt complexes with terphenyl diamide (TDA) ligands, where the central aromatic ring can interact with the metal center, to obtain novel low-coordinate, low-valent cobalt complexes. This work successfully yielded a low-valent cobalt bis-amide complex as crystals. Furthermore, pyridine and DMAP complexes were also obtained, revealing a relatively stronger stabilization effect from the aromatic ring.

This study provided valuable insights into the interaction between low-valent cobalt centers and aromatic rings. Notably, the TDA ligand system enabled cobalt to exhibit reversible Co(II)/Co(I) redox behavior, an unprecedented feature for low-coordinate cobalt amides. In addition, the Co(I) bisamide complexes were found to be thermally stable in both solution and solid states. Meanwhile, temperature-dependent crystallographic and theoretical analyses demonstrated that the cobalt center does not receive significant stabilization from the aromatic ring. While aromatic interactions commonly offer some stabilization, their effect on low-coordinate low-valent cobalt centers is limited, suggesting that these cobalt complexes may exhibit high reactivity. The reactivity of the Co(I) bis-amide complexes described in this study is currently under investigation and will be reported in future work.

Experimental Section

General Procedures: All manipulations were carried out under an argon atmosphere using standard Schlenk techniques and glove boxes unless otherwise stated. Dried solvents were purchased from Kanto Chemical Co. Inc. (for DME (ethylene glycol dimethyl ether), toluene, and hexane) and FUJIFILM Wako Pure Chemicals Co. (for THF). Et_2O was freshly distilled from Na/benzophenone ketyl. All the dried solvents were tested for H_2O and O_2 using a standard solution of potassium benzophenone ketyl radical anion, and kept over potassium and 4 Å molecular sieves. Benzene-d_6 and THF-d_8 were dried and degassed over a potassium mirror, and vacuum transferred prior to use. Elemental analyses were performed on Yanaco MT-6 microanalyzers. Cyclic voltammograms were recorded on a BSA-612E electrochemical analyzer using a Au working electrode and 0.2 M $(Bu_4N)(PF_6)$ as the supporting electrolyte. All samples were prepared at a concentration of 0.2 mM and measurements were performed under argon atmosphere at room temperature. ^{1}H and ^{13}C{^{1}H} NMR spectra were acquired on a JEOL ECS 400 or ECA 500. The ^{1}H NMR signals were referenced to the residual proton peak of the deuterated solvent. The ^{13}C chemical shifts were relative to the carbon signals for the deuterated solvents. The data were corrected at room temperature. Temperature-dependent magnetic DC susceptibility of microcrystalline samples, sealed in a quartz tube with small amount of Helium gas, were collected on a Quantum Design MPMS-XL7AC SQUID magnetometer in the range from 300 to 2.0 K under a dc magnetic field of 1.0 T. The experimental data were corrected by using Pascal's constant.[32] The experimental data were simulated by assuming the spin Hamiltonian:

$$\hat{\mathcal{H}} = \mu_B \vec{B}\boldsymbol{g}\vec{S} + D\left[\hat{S}_z^2 - \frac{1}{3}S(S+1)\right]$$

where μ_B is the Bohr magneton, $\vec{B}$ is a magnetic flux density, g is the g-tensor, D is the uniaxial zero-field splitting parameter, $\vec{S}$ is the spin operator, $\hat{S}_z$ is the z-component of spin operator, and S is the spin quantum number. The powder magnetization $M(B,T)$ is evaluated with conventional powder average procedure using 43-point Lebedev grid. For every magnetic field direction, spin energy eigenvalues and directional magnetizations were obtained by full-matrix diagonalization of the spin Hamiltonian. Model parameters were optimized by using the built-in nonlinear least squares algorithm of IGOR Pro. Infrared spectra were recorded on a Themo Scientific Nicolet iS5 FT-IR spectrometer. 2,4,6-Trimethylaniline ($MesNH_2$), 2,6-diisopropylaniline ($DippNH_2$), and 15-crown-5 ether (denoted as 15-crown-5 or 15-c-5) were dried and degassed over a CaH_2 (for aniline) or a potassium mirror (for crown ether), and vacuum transferred prior to use. KC_8 was prepared by heating potassium and graphite at 150 °C under an argon atmosphere. Other chemicals were used as received.

Synthesis of N^2,N$^{2''}$-bis(2,4,6-trimethylphenyl)-[1,1′:3′,1″-terphenyl]-2,2″-diamine (H_2TDA^{Mes}): Synthetic procedures and spectral data of 2,2″-dibromo-1,1′:3′,1″-terphenyl (TDBr) and H_2TDA^{Mes} have been already reported.[14,13] TDBr was prepared according to the literature procedure, and H_2TDA^{Mes} was prepared with modified method as below: In a 100 mL PTFE-stoppered flask were introduced $PdCl_2$ (1.3 mol%, 41 mg, 0.23 mmol), DPEPhos (2.0 mol%, 192 mg, 0.356 mmol), 2,4,6-trimethylaniline (2.4 eq., 5.9 mL, 42 mmol), and toluene (3 mL) under an argon atmosphere. The mixture was heated up to 80 °C for 2 hours, during which time a yellow precipitate was formed. After the mixture was cooled to room temperature, toluene (40 mL) was added to the solution, followed by addition of TDBr (1 eq., 6.79 g, 17.5 mmol). The mixture was stirred for 15 minutes, then sodium *tert*-butoxide (2.9 eq., 4.87 g, 50.7 mmol) was added. The resulting reddish-brown suspension was stirred at 100 °C for 48 hours. The reaction mixture was allowed to cool to room temperature, then water (20 mL) was added to quench the reaction under an open-air atmosphere. After the solvent was carefully removed under reduced pressure, the water (100 mL) was added to the residue, and aqueous layer was extracted with dichloromethane (3 × 100 mL). The organic layer was washed with water (100mL) and brine (100 mL), dried over anhydrous $MgSO_4$, filtered, and evaporated. The resulting brown oil was passed through a short column of silica gel with dichloromethane as eluent. After the solvent was removed on a rotary evaporator, a large amount of hexane (ca. 150 mL) was added to give H_2TDA^{Mes} as pale-yellow crystals in 70% yield (6.13 g, 12.3 mmol).

Synthesis of N^2,N$^{2''}$-bis(2,6-diisopropylphenyl)-[1,1′:3′,1″-terphenyl]-2,2″-diamine (H_2TDA^{Dipp}): H_2TDA^{Dipp} was prepared by following a similar procedure to that for H_2TDA^{Mes}. The reaction was carried out with $PdCl_2$ (1.3 mol%, 39 mg, 0.22 mmol), DPEPhos (2.0 mol%, 189 mg, 0.351 mmol), 2,6-diisopropylaniline (2.4 eq., 7.9 mL, 42 mmol), 2,2″-Dibromo-1,1′:3′,1″-terphenyl (1 eq., 6.80 g, 17.5 mmol), and sodium *tert*-butoxide (2.9 eq., 4.72 g, 49.1 mmol). The titled compound was isolated as colorless crystals in 37% yield (4.32 g, 7.44 mmol).

Synthesis of [K(15-crown-5)$_2$][(TDA^{Mes})Co^{II}Cl] (1): H_2TDA^{Mes} (102 mg, 0.205 mmol) was dissolved in THF (15 mL) and $KN(SiMe_3)_2$ (82 mg, 0.41 mmol) was added to the solution. The mixture was stirred for 1 h, and then the solvent was removed under reduced pressure. The orange residue was dissolved in DME and $CoCl_2$ (27 mg, 0.21 mmol) was added to the solution to give a reddish-brown solution. The reaction mixture was stirred for 1.5 h, and then filtered and concentrated to *ca*. 3 mL to give reddish-brown solution. 15-crown-5 ether (99 mg, 0.45 mmol) was added to the solution followed by addition of *n*-Hexane (*ca*. 1 mL), and the solution was cooled to –30 °C to give **1** as reddish-brown crystals in 74% yield (176 mg, 0.152 mmol).

Synthesis of [K(15-crown-5)$_2$][(TDA^{Dipp})Co^{II}Cl] (2): H_2TDA^{Dipp} (73 mg, 0.13 mmol) was dissolved in THF (15 mL) and $KN(SiMe_3)_2$ (51 mg, 0.25 mmol) was added to the solution. The mixture was stirred for 1 h, and then the solvent was removed under reduced pressure. The orange residue was dissolved in 1,2-dimetoxyethane (DME) and $CoCl_2$ (17 mg, 0.13 mmol) was added to the solution to give a reddish-brown solution. After 4 h stirring, the reaction mixture was filtered and concentrated to ca. 5 mL to give reddish-brown solution. 15-cronwn-5 ether (62 mg, 0.28 mmol) was added to the solution, and the solution was stored at ambient temperature to give **2** as reddish-brown crystals in 60% yield (97 mg, 0.078 mmol).

Synthesis of (TDA^{Mes})Co^{II}THF (1′): To a solution of H_2TDA^{Mes} (181 mg, 0.364 mmol) in 10 mL of THF was added $KN(SiMe_3)_2$ (2.2 eq., 160 mg, 0.80 mmol), it immediately turned orange. After stirred for 1 h, $CoCl_2$ (47 mg, 0.36 mmol) was added to the solution. The mixture was stirred for 3 h, and then the solvent was removed under reduced pressure. The resulting residue was extracted with THF (7 mL) and centrifuged. The supernatant was concentrated to *ca.* 5 mL, hexane (*ca.* 1 mL) was added to the solution, and the solution was cooled at –35 °C to **1′** as reddish-brown crystals in 51% yield (117 mg, 0.187 mmol).

Synthesis of (TDA^{Dipp})Co^{II}THF (2′): Complex **2′** was prepared by following a similar procedure to that for **1′**. The reaction was carried out with H_2TDA^{Dipp} (151 mg, 0.260mmol), $KN(SiMe_3)_2$ (2.2 eq., 114 mg, 0.571 mmol), and $CoCl_2$ (34 mg, 0.26 mmol). The titled compound was isolated as reddish-brown crystals in 56% yield (104 mg, 0.147 mmol).

Synthesis of [K(15-crown-5)$_2$][(TDA^{Mes})Co^{I}] (3): Method A (from 1): To a DME (5 mL) solution of **1** (46 mg, 0.040 mmol) was added a DME suspension of KC_8 (5.9 mg, 0.044 mmol) under stirring, leading to a gradual color change from reddish-purple to greenish-brown. The reaction mixture was stirred for 1 h, and then filtered and concentrated to *ca*. 3 mL to give brown solution. *n*-Hexane (*ca*. 1 mL) was added to the solution,

and the solution was cooled to –30 °C to give **3** as brackish-brown crystals in 46% yield (19 mg, 0.018 mmol).

Method B (from 1'): To a DME (5 mL) solution of **1'** (266 mg, 0.425 mmol) was added a powder of KC_8 (63 mg, 0.47 mmol) at –30 °C. The reaction mixture was allowed to warm up to room temperature with stirring for 2 h, and centrifuged. The solution was then concentrated to *ca.* 10 mL under reduced pressure. Hexane (*ca.* 1 mL) and 15-crown-5 ether (186 mg, 0.860 mmol) were added to the solution, and the solution was cooled at –35 °C to give **3** as brownish-green crystals in 74% yield (327 mg, 0.320 mmol).

Method C (from H_2TDA^{Mes}): To a THF (10 mL) solution of H_2TDA^{Mes} (238 mg, 0.480 mmol) was added a powder of $KN(SiMe_3)_2$ (191 mg, 0.958 mmol). The mixture was stirred for 3 h, and then the solvent was removed. The orange residue was dissolved in THF and $CoCl_2$ (62 mg, 0.48 mmol) was added to the solution to give a reddish-brown solution. After overnight stirring, the reaction mixture was filtered and evaporated, followed by washing with *n*-hexane to give a reddish-brown powder. The powder was dissolved in DME (5 mL) and a powder of KC_8 (57 mg, 0.42 mmol) was added to the solution under stirring at –30 ℃, warmed up to r.t. leading to a gradual color change from reddish-brown to greenish-brown. The reaction mixture was stirred for 2 h, and then filtered and concentrated to *ca*. 3 mL to give greenish-brown solution. To the solution were added 15-crown-5 ether (190 mg, 0.860 mmol) and *n*-Hexane (*ca*. 1 mL), and then cooled to –30 °C to give **3** as dark brown crystals in 74% yield (367 mg, 0.355 mmol).

Synthesis of $[K(15\text{-crown-}5)_2][(TDA^{Dipp})Co^{I}]$ (4): Method A (from 2): In this method, complex **4** was prepared by following a similar procedure to **method A** for **3**. The reaction was carried out with **2** (90 mg, 0.072 mmol), KC_8 (10 mg, 0.072 mmol), and 15-crown-5 ether (35 mg, 0.16 mmol) in a THF solution. The titled compound was isolated as dark brown crystals in 46% yield (37 mg, 0.033 mmol).

Method B (from 2'): In this method, complex **4** was prepared by following a similar procedure to **method B** for **3**. The reaction was carried out with **2'** (57 mg, 0.080 mmol), KC_8 (12 mg, 0.089 mmol), and 15-crown-5 ether (35 mg, 0.16 mmol) in a THF solution. The titled compound was isolated as dark brown crystals in 73% yield (65 mg, 0.058 mmol).

Method C (from H_2TDA^{Dipp}): In this method, complex **4** was prepared by following a similar procedure to **method C** for **3**. The reaction was carried out with H_2TDA^{Dipp} (243 mg, 0.419 mmol), $KN(SiMe_3)_2$ (167 mg, 0.838 mmol), $CoCl_2$ (55.3 mg, 0.426 mmol), KC_8 (58 mg, 0.43 mmol), 15-crown-5 ether (189 mg, 0.860 mmol) in a THF solution. The titled compound was isolated as dark brown crystals in 84% yield (397 mg, 0.355 mmol).

Synthesis of $[K(15\text{-crown-}5)_2][(TDA^{Mes})Co^{I}(Py)]$ (5): To a THF (5 mL) solution of **3** (46 mg, 0.044 mmol) was added pyridine (18 µL, 0.22 mmol, 5.1 eq.) under stirring, leading to an gradual color change from greenish-brown to brown. The reaction mixture was stirred for 2 h, and then filtered and concentrated to *ca.* 3 mL to give brown solution. n-Hexane (*ca.* 1 mL) was added to the solution, and the solution was cooled to –30 °C to give **5** as dark brown crystals in 56% yield (27 mg, 0.025 mmol).

Synthesis of $[K(15\text{-crown-}5)_2][(TDA^{Mes})Co^{I}(DMAP)]$ (6): To a DME (5 mL) solution of **3** (45 mg, 0.043 mmol) was added a DME solution of DMAP (6.0 mg, 0.049 mmol) under stirring, leading to an gradual color change from greenish-brown to brown. The reaction mixture was stirred for 7 hours, and then filtered and concentrated to *ca*. 3 mL to give brown solution. The solution was cooled to –30 °C to give **6** as dark brown crystals in 54% yield (29 mg, 0.023 mmol).

X-ray crystallographic study: Intensity data for single-crystal X-ray structure determination were collected using a Rigaku XtaLAB Synergy Custom (Detector: Hypix-6000HE) or a Rigaku R-AXIS RAPID 191R diffractometer with Mo-Kα radiation (λ = 0.71073 Å). Measurement, data reduction, and absorption correction were performed with CrysAlisPro[33] or Rigaku Rapid Auto[34] program package. Structure solution and refinement were performed with the Olex2 ver. 1.5 software package.[35] All structures were solved by intrinsic phasing method within SHELXT program[36] or charge flipping method within olex2.solve program[37], and refined on F^2 by the full-matrix least-square technique using version 2018/3 of ShelXL[38]. The details of each crystal structure are provided on page S-31 of the Supporting Information.

Acknowledgments

This research was financially supported by Grant-in-Aids for Scientific Research(C) (Nos. JP16K05720 and JP20K05527) from the Ministry of Education, Culture, Sports, Science and Technology (MEXT) of Japan. All measurements for single crystal X-ray diffraction, NMR spectroscopy, and elemental analysis were performed at the Analytical Instrument Facility, Graduate School of Science, Osaka University. These research equipments are shared in MEXT Project for promoting public utilization of advanced research infrastructure (Program for supporting construction of core facilities) (No. JPMXS0441200021–JPMXS0441200024). We thank Mr. Ken-ichi Iijima and Ms. Tomomi Hirai (Osaka University) for assistance with elemental analysis. The theoretical calculations were performed using the Research Center for Computational Science, Okazaki, Japan.

Conflict of Interests

The authors declare no conflict of interest.

Data Availability Statement

The data that support the findings of this study are available in the supplementary material of this article. Deposition Numbers 2408279 (for **1**·DME), 2408274 (for **2**·DME), 2408267 (for **1'**), 2408265 (for **2'**·0.25THF), 2408271 (for **3** at 113 K), 2408276 (for **3** at 173 K), 2408266 (for **3** at 223 K), 2408273 (for **4**·2THF at 113 K), 2408268 (for **4**·2THF at 173 K), 2408277 (for **4**·2THF at 223 K), 2408275 (for **4'**·0.5Et_2O), 2408278 (for **5** at 113 K), 2408272 (for **5** at 173 K), 2408270 (for **5** at 223 K), and 2408269 (for **6**·DME) contain the supplementary crystallographic data for this paper. These data are provided free of charge by the joint Cambridge Crystallographic Data Centre and Fachinformationszentrum Karlsruhe Access Structures service.

Keywords: Transition metals • Reduction • N ligands • Arene ligands • Donor-acceptor systems

[1] P. Gandeepan, T. Müller, D. Zell, G. Cera, S. Warratz, L. Ackermann, *Chem. Rev.* **2019**, 2192–2452.

[2] a) G. Cahiez, A. Moyeux, *Chem. Rev.* **2010**, *110*, 1435–1462; b) K. Gao, N. Yoshikai, *Acc. Chem. Res.* **2014**, *47*, 1208–1219; c) N. Yoshikai, *Bull. Chem. Soc. Jpn.* **2014**, *87*, 843–857; c) L. Ackermann, *J. Org. Chem.* **2014**, *79*, 8948–8954; d) M. Moselage, J. Li, L. Ackermann, *ACS Catal.* **2016**, *6*, 498–525; e) M. M. Tohidi, B.Paymard, S. R. Vasquez-García, D. Fernández-Quiroz, *Tetrahedron* **2023**, *136*, 133352; f) S. Hassan, M. Bilal, S. Khalid, N. Rasool, M. Imran, A. A. Shah, *Mol. Divers.* **2024**, https://doi.org/10.1007/s11030-024-11017-1.

[3] P. P. Power, *Chem. Rev.* **2012**, *112*, 3482–3507.

[4] C.-Y. Lin, J. C. Fettinger, F. Grandjean, G. J. Long, P. P. Power, *Inorg. Chem.* **2014**, *53*, 9400–9406.

[5] J. Hicks, C. Jones, *Organometallics* **2015**, *34*, 2118–2121;

[6] a) C. G. Werncke, E. Suturina, P. C. Bunting, L. Vendier, J. R. Long, M. Atanasov, F. Neese, S. Sabo-Etinne, S. Bontemps, *Chem. Eur. J.* **2016**, *22*, 1668–1674; b) T. Hatanaka, Y. Funahashi, *CSD Communication* **2024**, refcode: MUNYAZ.

[7] a) Y. Liu, L. Deng, *J. Am. Chem. Soc.* **2017**, *139*, 1798–1801; b) A. A. Danopoulos, P. Braunstein, K. Y. Monakhov, J. van Leusen, P. Kögerler,

M. Clémancey, J.-M. Latour, A. Benayad, M. Tromp, E. Rezabal, G. Frison, *Dalton Trans.* **2017**, *46*, 1163–1171.

[8] A. Nicolay, M. S. Zieglar, L. Rochlitz, T. D. Tilley, *Polyhedron* **2020**, *180*, 11420.

[9] Y. Dong, M. I. Lipschutz, R. J. Witzke, J. A. Panetier, T. D. Tilley, *ACS Catal.* **2021**, *11*, 11160– 11170.

[10] R. Weller, L. Ruppach, A. Shlyaykher, F. Tambornino, C. G. Werncke, *Dalton Trans.* **2021**, *50*, 10947–10963.

[11] a) I. Müller, C. Schneider, C. Pietzonka, F. Kraus, C. G. Werncke, *Inorganics* **2019**, *7*, 117; b) Al. Reckziegel, C. Pietzonka, F. Kraus, C. G. Werncke, *Angew. Chem. Int. Ed.* **2020**, *59*, 8527–8531; c) I. Müller, D. Munz, C. G. Werncke, *Inorg. Chem.* **2020**, *59*, 9521–9537; d) A. Reckziegel, M. Kour, B. Battistella, S. Mebs, K. Beuthert, R. Berger, C. G. Werncke, *Angew. Chem. Int. Ed.* **2021**, *60*, 15376–15380; e) R. Weller, I. Müller, C. Duhayon, S. Sabo-Etienne, S. Bontemps, C. G. Werncke, *Dalton Trans.* **2021**, *50*, 4890–4903; f) R. Weller, L. Völlinger, C. G. Werncke, *Eur. J. Inorg. Chem.* **2021**, *42*, 4383–4392; g) I. Müller, C. G. Werncke, *Chem. Eur. J.* **2021**, 27, 4932–4938; h) G. Sieg, Q. Pessemesse, S. Reith, S. Yelin, C. Limberg, D. Munz, C. G. Werncke, *Chem. Eur. J.* **2021**, *27*, 16760–16767; i) C. Schneider, L. Guggolz, C. G. Werncke, *Dalton Trans.* **2022**, *51*, 179–184.

[12] a) F. Paul, J. Patt, J. F. Hartwig, *J. Am. Chem. Soc.* **1994**, *116*, 5969–5970; b) A. S. Guram, S. L. Buchwald, *J. Am. Chem. Soc.* **1994**, *116*, 7901–7902.

[13] A. S. Veige, J. M. Falkowski, M. O'Reilly, S. Kuppuswamy, K. P. McGowan, S. Sarkar, (University of Florida Research Foundation, Inc.), WO 2010/101993, **2010**.

[14] S. T. Chao, N. C. Lara, S. Lin, M. W. Day, T. Agapie, *Angew. Chem. Int. Ed.* **2011**, *50*, 7529–7532.

[15] a) A. Cetin, W. S. Durfee, C. J. Ziegler, *Inorg. Chem.* **2007**, *46*, 6239–6241; b) J. Hicks, C. Jones, *Inorg. Chem.* **2013**, *52*, 3900–3907; c) G. A. Edouard, P. Kelley, D. E. Herbert, T. Agapie, *Organometallics* **2015**, *34*, 5254–5277; d) Y. Baek, E. T. Hennessy, T. A. Betley, *J. Am. Chem. Soc.* **2019**, *141*, 16944–16953.

[16] L. Yang, D. R. Powell, R. P. Houser, *Dalton Trans.* **2007**, 955–964.

[17] M. M. Olmstead, P. P. Power, B. M. Murray, *CSD Communication* **2018**, refcode: AGANOO.

[18] A. M. Bryan, G. J. Long, F. Grandjean, P. P. Power, *Inorg. Chem.* **2013**, *52*, 12152–12160.

[19] S. N. König, C. Schädle, C. Maichle–Mössmer, R. Anwander, *Inorg. Chem.* **2014**, *53*, 4585–4597.

[20] a) I. Čorić, B. Q. Mercado, E. Bill, D. J. Vinyard, P. L. Holland, *Nature* **2015**, *526*, 96–99; b) A. L. Speelman, I. Čorić, C. V. Stappen, S. DeBeer, B. Q. Mercado, P. L. Holland, *J. Am. Chem. Soc.* **2019**, *141*, 13148–13157.

[21] a) S. T. Chao, N. C. Lara, S. Lin, M. W. Day, T. Agapie, *Angew. Chem. Int. Ed.* **2011**, *50*, 7529–7532; b) P. Kelley, S. Lin, G. Edouard, M. W. Day, T. Agapie, *J. Am. Chem. Soc.* **2012**, *134*, 5480–5483; c) D. E. Herbert, N. C. Lara, T. Agapie, *Chem. Eur. J.* **2013**, *19*, 16453–16460; d) G. A. Edouard, P. Kelley, D. E. Herbert, T. Agapie, *Organometallics* **2015**, *34*, 5254–5277.

[22] W. Steffen, T. Blömker, N. Kleigrewe, G. Kehr, R. Fröhlich, G. Erker, *Chem. Commun.* **2004**, 1188–1189.

[23] K. Tokmic, B. J. Jackson, A. Salazar, T. J. Woods, A. R. Fout, *J. Am. Chem. Soc.* **2017**, *139*, 13554–13561.

[24] a) J. J. Ellison, P. P. Power, *J. Organomet. Chem.* **1996**, *526*, 263–267; b) S. Yoshimitsu, S. Hikichi, M. Akita, *Organometallics* **2002**, *21*, 3762–3773; c) A. D. Sutton, T. Ngyuen, J. C. Fettinger, M. M. Olmstead, G. J. Long, P. P. Power, *Inorg. Chem.* **2007**, *46*, 4809–4814; d) T. Zheng, H. Sun, Y. Chen, X. Li, S. Dürr, U. Radius, K. Harms, *Organometallics* **2009**, *28*, 5771–5776; e) C. Ni, G. J. Long, F. Grandjean, P. P. Power *Inorg. Chem.* **2009**, *48*, 11594–11600; f) J. Li, T. Zheng, H. Sun, W. Xu, X. Li, *Dalton Trans.* **2013**, *42*, 5740–5748; g) R. R. Reinig, E. L. Fought, A. Ellern, T. L. Windus, A. D. Sadow, *Dalton Trans.* **2018**, *47*, 12147–12161.

[25] a) R. Diercks, B. E. Eaton, S. Gürtzgen, S. Jalisatgi, A. J. Matzger, R. H. Radde, K. P. C. Vollhardt, *J. Am. Chem. Soc.* **1998**, *120*, 8247–8248; b) J. J. Schneider, D. Wolf, C. W. Lehmann, *Inorg. Chim. Acta* **2003**, *350*, 625–632; c) W. W. Brennessel, V. G. Young Jr., J. E. Ellis, *Angew. Chem. Int. Ed.* **2006**, *45*, 7268-7271; d) S. Guo, R. Hauptmann, J. J. Schneider, *Z. Anorg. Allg. Chem.* **2007**, *633*, 2332–2337; e) X. Wang, Y. Zhao, S. Gong, B. Liu, Q.-S. Li, J.-H. Su, B. Wu, X.-J. Yang, *Chem. Eur. J.* **2015**, *21*, 13302–13310; f) D. Ertler, M. W. Kuntze-Fechner, S. Dürr, K. Lubitz, U. Radius, *New J. Chem.* **2021**, *45*, 14999–15016;

[26] a) J. J. Schneider, U. Denninger, O. Heinemann, C. Krüger, *Angew. Chem. Int. Ed.* **1995**, *34*, 592–595; b) H. Wadepohl, K. Büchner, M. Herrmann, A. Metz, H. Pritzkow, *J. Organomet. Chem.* **1998**, *571*, 267–278; c) H. Wadepohl, K. Buechner, M. Herrmann, H. Pritzkow, *Organometallics* **1991**, *10*, 861–871; d) H. Wadepohl, T. Borchert, H. Protzkow, *J. Organomet. Chem.* **1996**, *516*, 187–189; e) H. Wadepohl, M. J. Calhorda, M. Herrmann, C. Jost, P. E. M. Lopes, H. Pritzkow, *Organometallics* **1996**, *15*, 5622–5634; f) K. T. Horak, A. Velian, M. W. Day, T. Agapie, *Chem. Commun.* **2014**, *50*, 4427–4429.

[27] a) R. F. W. Bader, *Acc. Chem. Res.* **1985**, *18*, 9–15; b) R. F. W. Bader, *Chem. Rev.* **1991**, *91*, 893–928; c) R. F. W. Bader, *Atoms in Molecules: A Quantum Theory*, Oxford University Press: Oxford, UK, **1990**.

[28] K. B. Wiberg, *Tetrahedron* **1968**, *24*, 1083–1096.

[29] a) I. Mayer, *Chem. Phys. Lett.* **1983**, *97*, 270–274; b) I. Mayer, *J. Comput. Chem.* **2007**, *28*, 204–221.

[30] A. E. Reed, L. A. Curtiss, F. Weinhold, *Chem. Rev.* **1988**, *88*, 899–926.

[31] a) M. L. H. Green, *J. Organomet. Chem.* **1995**, *500*, 127–148; b) G. Parkin, *Organometallics* **2006**, *25*, 4744–4747; c) H. Braunschweig, R. D. Dewhurst, A. Schneider, *Chem. Rev.* **2010**, *110*, 3924–3957; d) A. Amgoune, D. Bourissou, *Chem. Commun.* **2011**, *47*, 859–871; e) H. Kameo, H. Nakazawa, *Chem. Asian J.* **2013**, *8*, 1720–1734; f) J. S. Jones, F. P. Gabbaï, *Acc. Chem. Res.* **2016**, *49*, 857–867; g) G. Bouhadir, D. Bourissou, *Chem. Soc. Rev.* **2016**, *45*, 1065–1079; h) R. C. Cammarota, L. J. Clouston, C. C. Lu, *Coord. Chem. Rev.* **2017**, *334*, 100–111; i) D. You, F. P. Gabbaï, *Trends Chem.* **2019**, *1*, 485–496.

[32] G. A. Bain, J. F. Berry, *J.Chem. Educ.* **2008**, *85*, 532–536.

[33] CrysAlisPro Software System ver. 1.171.41.122a. Rigaku Oxford Diffraction, 2021.

[34] Rigaku's Rapid Auto System. Rigaku corporation, 1998.

[35] O. V. Dolomanov, L. J. Bourhis, R. J. Gildea, J. A. K. Howard, H. Puschmann, *J. Appl. Cryst.* **2009**, *42*, 339–341.

[36] G. M. Sheldrick, *Acta Cryst.* **2015**, *A71*, 3–8.

[37] L. J. Bourhis, O. V. Dolomanov, R. J. Gildea, J. A. K. Howard, H. Puschmann, *Acta Cryst.* **2015**, *A71*, 59–75.

[38] G. M. Sheldrick, *Acta Cryst.* **2015**, *C71*, 3–8.

Entry for the Table of Contents

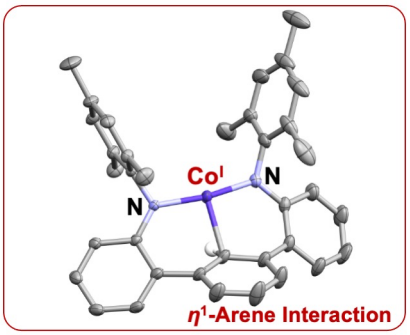

Novel low-coordinate Co(I) bisamide complexes featuring η^1-arene interaction were synthesized and characterized. These complexes exhibit significant Co–C bond shortening upon one-electron reduction or N-donor ligation, offering new insights into cobalt–aromatic interactions and electronic structures of low-coordinate low-valent amide complexes.